Computational Analysis of the External Aerodynamics of the Unpowered X-57 Mod-III Aircraft

Presented at 2019 AIAA AVIATION, June 21th 2019

Seung Y. Yoo
NASA Armstrong Flight Research Center

Jared C. Duensing
NASA Ames Research Center

Acknowledgement

- NASA Armstrong Team
  - Mike Frederick, Nicholas Johnson, Trong Bui, Thomas Matthews
- NASA Ames Team
  - Daniel Maldonado, Jeffrey A. Housman, James C. Jensen, Cetin C. Kiris
- NASA Langley Team
  - Karen A. Deere, Jeffrey K. Viken, Melissa B. Carter, Sally A. Viken

Outline

- Introduction
- Method
- Results
- Conclusion
- Questions

Introduction

- X-57 Program
  - Separated into multiple phases, denoted as “MOD”, to demonstrate various technologies
    - Electrical power-plant
    - Optimized high aspect ratio wing and high lift nacelle
    - Tip cruise motor for reducing induced drag
- Study focused on unpowered MOD-III
  - flow physics
  - differences in flow solution between CFD solvers
- Purpose of the study
  - Aerodynamic database generation for pilot-in-the-loop simulation
  - Understanding of the aerodynamics of the vehicle for flight safety
  - Baseline performance for powered simulation

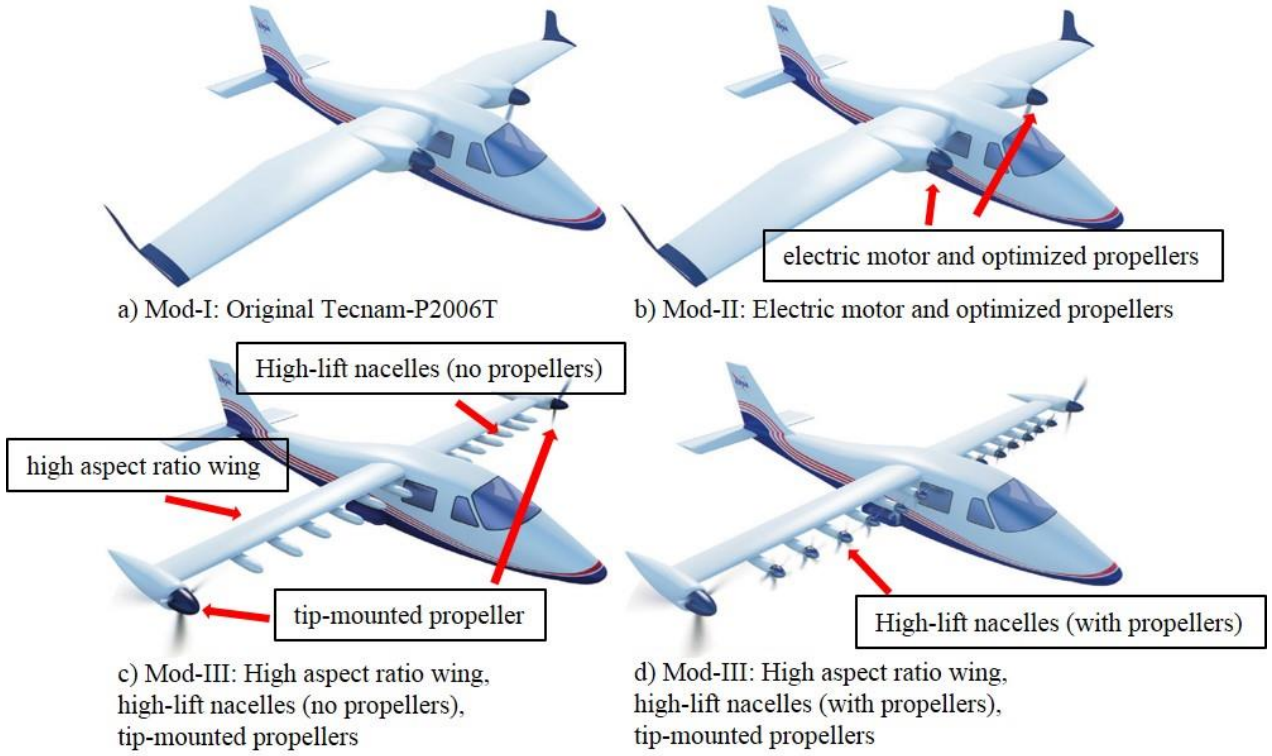

a) Mod-I: Original Tecnam-P2006T

b) Mod-II: Electric motor and optimized propellers

c) Mod-III: High aspect ratio wing, high-lift nacelles (no propellers), tip-mounted propellers

d) Mod-III: High aspect ratio wing, high-lift nacelles (with propellers), tip-mounted propellers

Method

- STAR-CCM+ (v13.04.10)
  - Used extensively at NASA AFRC for airworthiness analysis
  - Grid
    - Unstructured polyhedral mesh
    - Half-span with symmetry boundary condition for symmetric flow, full-span for asymmetric flow simulation
  - Solver
    - Steady state RANS
    - 2nd order Roe flux differencing scheme with algebraic multigrid solver with Gauss-Siedel relaxation scheme
    - Fully turbulent assumption, Spalart-Allmaras with rotational correction

- Launch Ascent Vehicle Analysis Framework
  - Versatile NASA ARC developed framework consisting of multiple solvers
  - Grid
    - Overset, structured, curvilinear grids
    - Full-span for all simulations
  - Solver
    - Steady state RANS structured curvilinear solver
    - Second-order convective flux with Koren limiter
    - Fully turbulent flow assumption, Spalart-Allmaras turbulence rotational correction and quadratic constitutive relationship

Result

- Grid Refinement Study
- Angle of attack sweep
- Sideslip angle sweep

Result – Grid Refinement Study

- Atmospheric Condition
  - Altitude 2500 ft, Mach 0.139, freestream velocity = 153.87 ft/s
  - density 2.2078E-3kg/m^3, static pressure = 1931.9 lbf/ft^2, static temperature 283.2K
  - Reynolds number 9.21E5
  - Angle of attack = 10°,Sideslip angle = 20°
- Aircraft configuration
  - Aileron = -25°
  - Flap = 30°
  - Rudder = -28°
  - Stabilator = -15°
  - Pitch trim tab = -18°

Result – Grid Refinement Study

- STAR-CCM+ Polyhedral Grid (coarse grid shown for clarity)

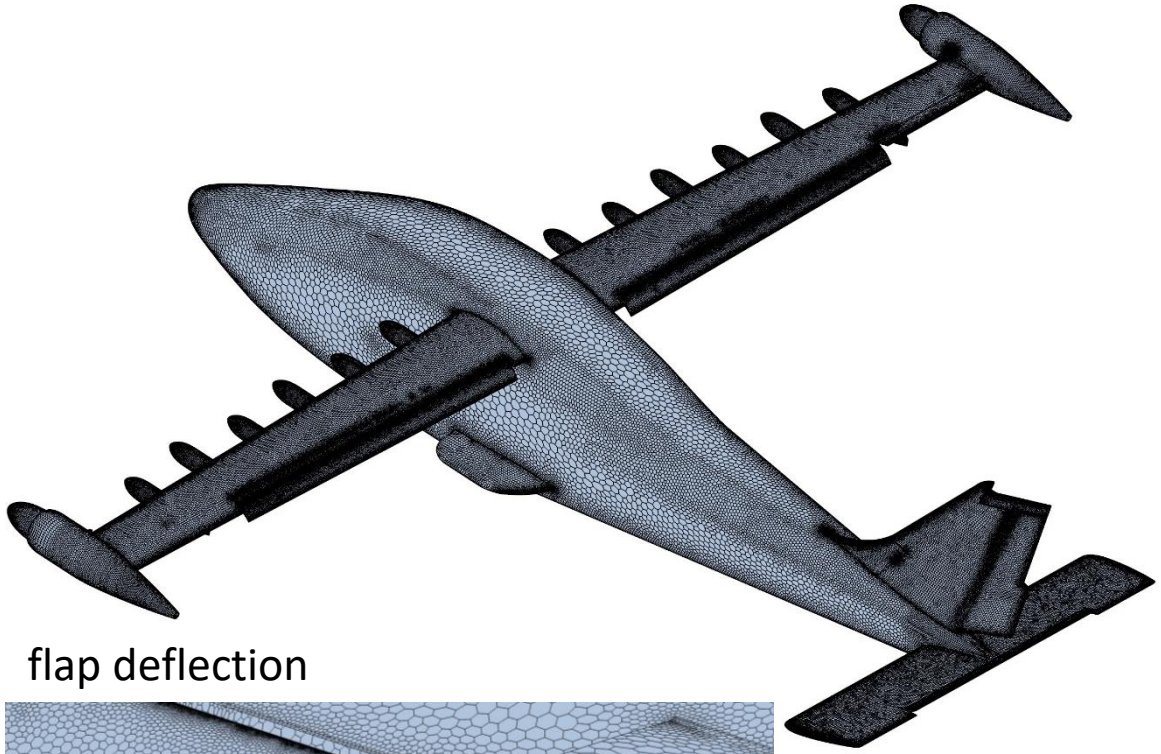

high lift nacelle

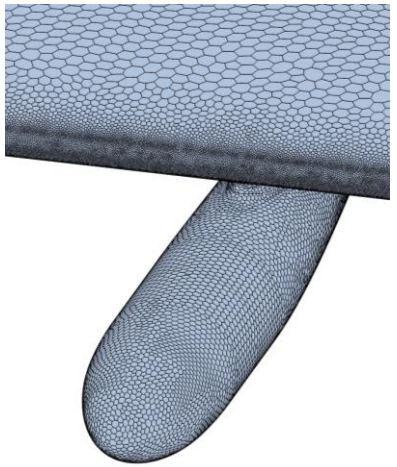

rudder deflection

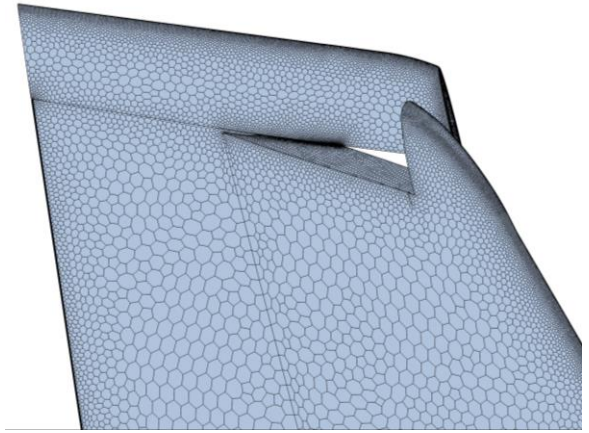

flap deflection

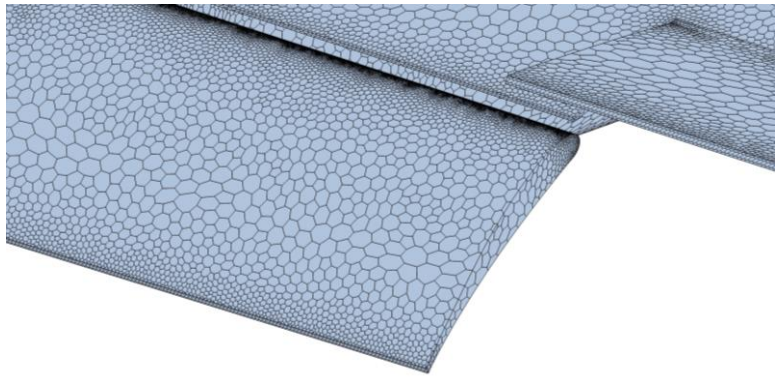

pitch trim tab on stabilator

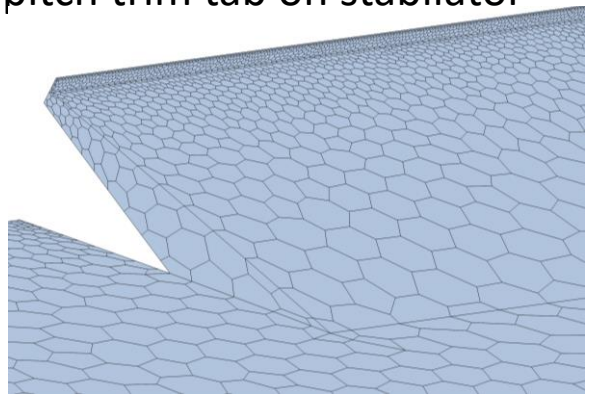

stabilator

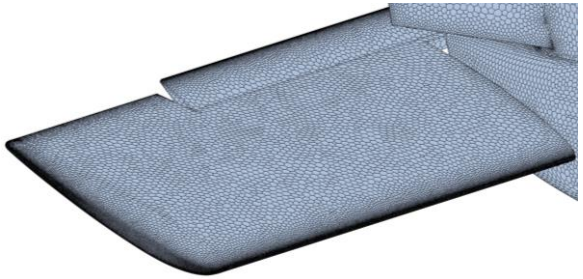

Result – Grid Refinement Study

- LAVA structured overset curvilinear grid (coarse grid shown for clarity)

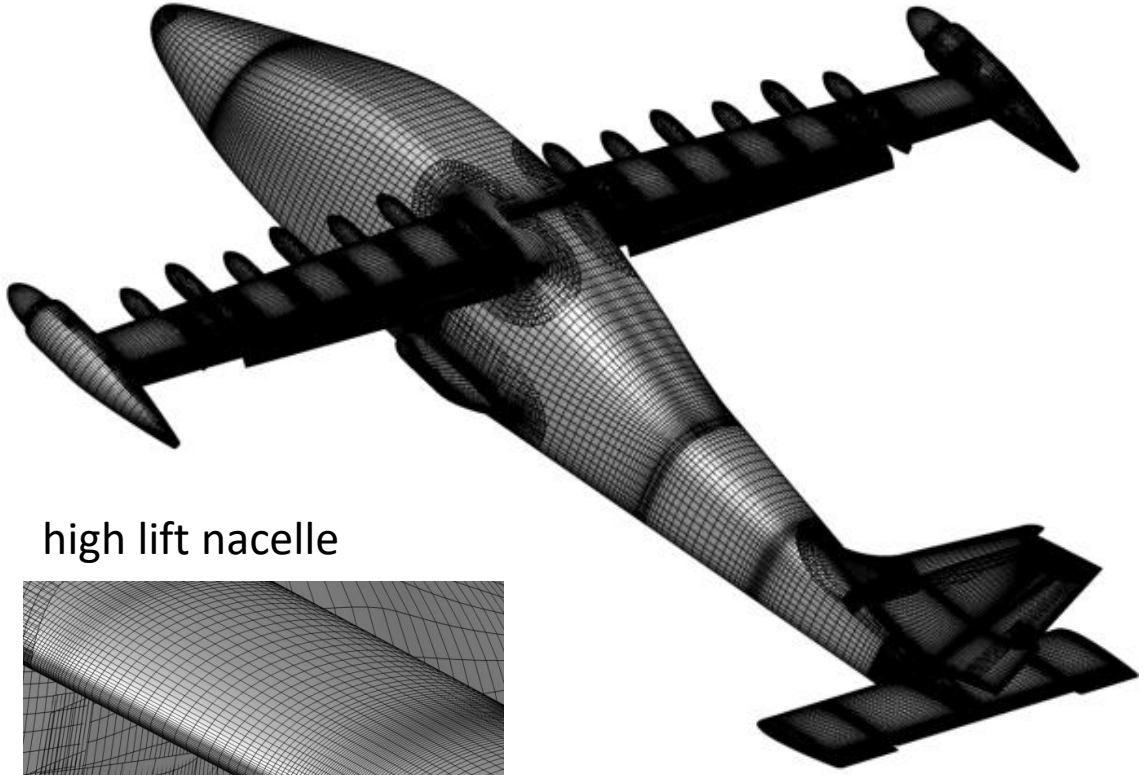

high lift nacelle

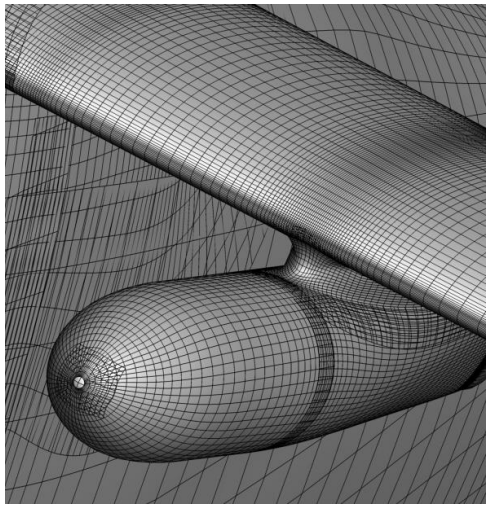

pitch trim tab on stabilator

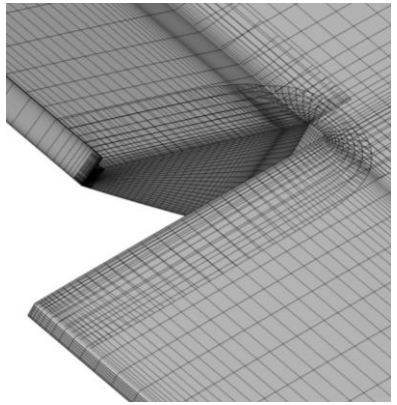

stabilator

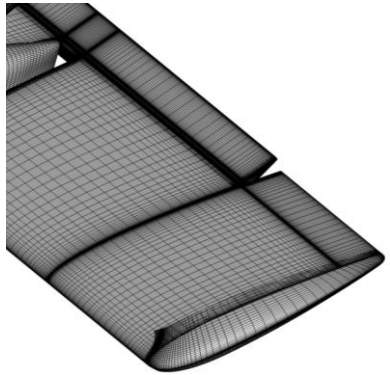

flap and rudder deflection

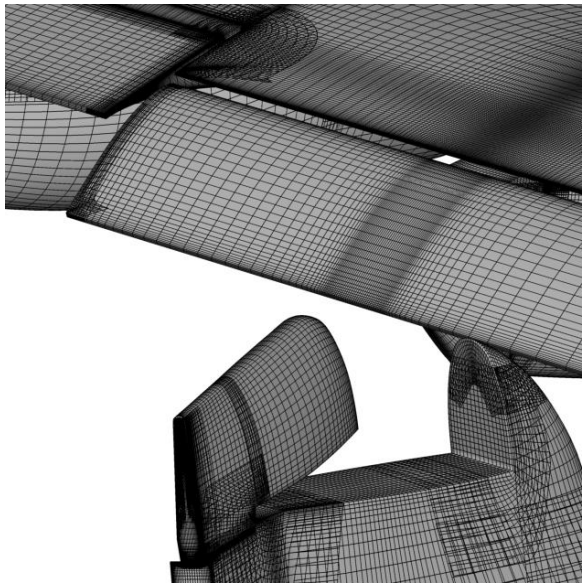

Result – Grid Refinement Study

- STAR-CCM+
  - 3 resolutions: 45e6 Cells (coarse), 77e6 Cells (medium), 126e6 Cells (fine)
- LAVA
  - 5 resolutions: 60.1e6 nodes (coarse), 95.2e6 nodes (medium), 248.6e6 nodes (fine), 312.6e6 nodes (very-fine), 425.7e6 nodes (extra-fine)

Result – Grid Refinement Study

STAR-CCM+ grid resolution	C_D	C_L	C_Y	C_l	C_m	C_n
coarse (45e6 cells)	**0.30394**	**1.46749**	**-0.61327**	**0.01631**	**2.41895**	**0.12050**
medium (77e6 cells)	0.30623	1.47778	-0.61585	0.02004	2.41327	0.12257
fine (126e6 cells)	0.30797	1.47193	-0.61886	0.01982	2.38941	0.12337

STAR-CCM+ grid resolution	C_D error, %	C_L error, %	C_Y error, %	C_l error, %	C_m error, %	C_n error, %
coarse (45 mil. cell)	**-1.1**	**-0.3**	**-0.9**	**-17.7**	**1.2**	**-2.3**
medium (77 mil. cell)	-0.5	0.4	-0.5	1.1	1.0	-0.6

Although relative error C_l is large, the values are small and coarse mesh chosen to accommodate the large number of runs for limited computing resource

Result – Grid Refinement Study

LAVA grid resolution	C_D	C_L	C_Y	C_l	C_m	C_n
coarse (60.1 mil. nodes)	0.3024	1.57	-0.6053	0.0135	2.396	0.1119
medium (95.2 mil. nodes)	0.29838	1.55	-0.595	0.016	2.404	0.1117
fine (248.6 mil. nodes)	**0.30036**	**1.56**	**-0.5876**	**0.0181**	**2.398**	**0.1106**
very-fine (312.6 mil. nodes)	0.30265	1.56	-0.5844	0.0226	2.402	0.1121
extra-fine (425.7 mil nodes)	0.30237	1.56	-0.582	0.0239	2.401	0.1126

LAVA grid resolution	C_D error, %	C_L error, %	C_Y error, %	C_l error, %	C_m error, %	C_n error, %
coarse (60.1 mil. nodes)	-0.01	-0.64	-4.00	43.51	0.21	0.62
medium (95.2 mil. nodes)	1.32	0.51	-2.23	33.05	-0.12	0.80
fine (248.6 mil. nodes)	**0.66**	**-0.26**	**-0.96**	**24.27**	**0.12**	**1.78**
very-fine (312.6 mil. nodes)	-0.09	-0.32	-0.41	5.44	-0.04	0.44

Result – Grid Refinement Study

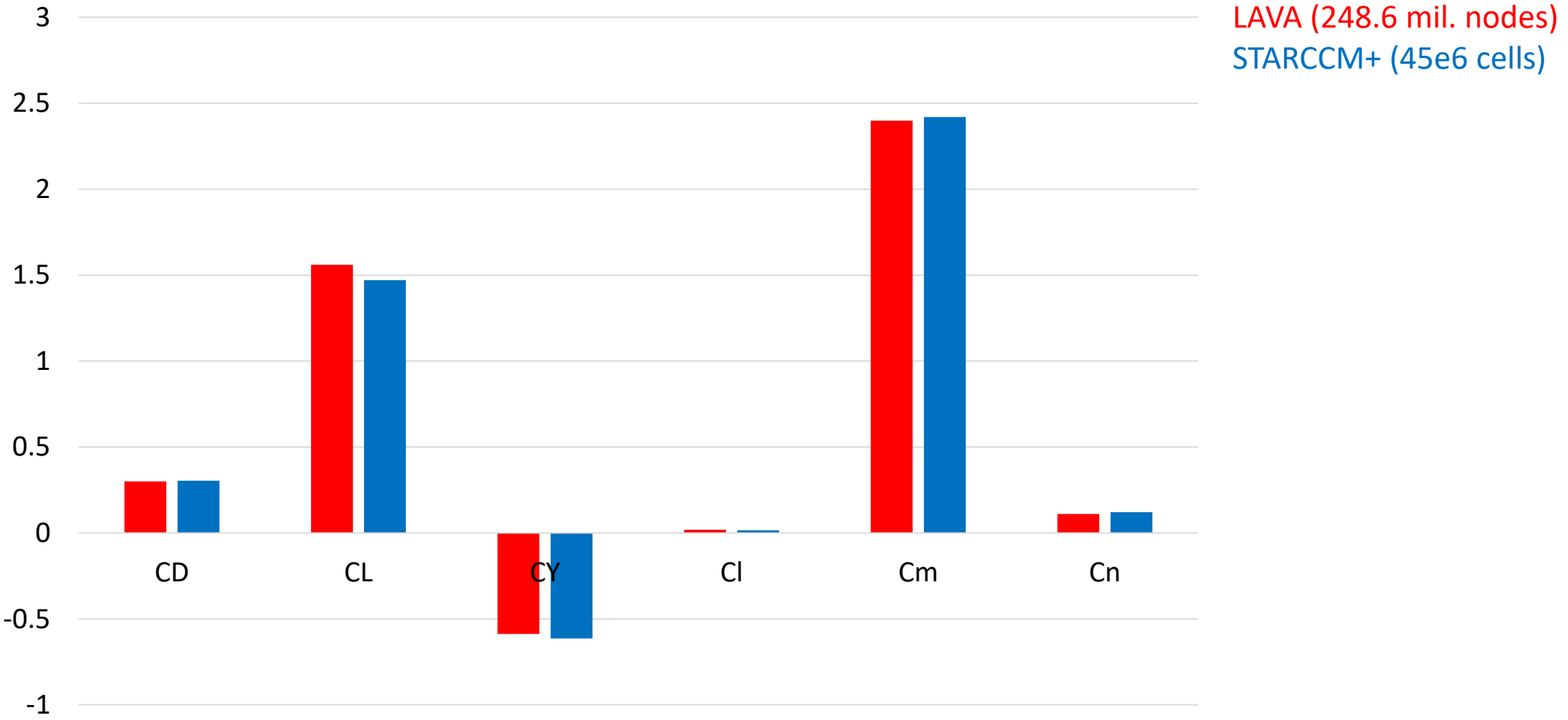

Result

- Grid Refinement Study
- Angle of attack sweep
- Sideslip angle sweep

Result – Angle of attack sweep

- 3 flap settings – 0° (cruise) , 10° (take-off), 30° (landing)
- Control surfaces in neutral position (no deflection)

	Flap = 0°	**Flap = 10°**	**Flap = 30°**
Altitude, ft	8000	2500	2500
Mach	0.233	0.149	0.139
Density, slug/ft^3	1.8628E-3	2.20782E-3	2.20782E-3
Static pressure, lbf/ft^2	1571.9	1931.9	1931.9
Static temperature, K	272.3	283.2	283.2
Coefficient of viscosity, slug/ft/s	3.57532E-7	3.68708E-7	3.68708E-7
Reynolds number	1.32E6	9.875E5	9.21E5

Result – Angle of attack sweep

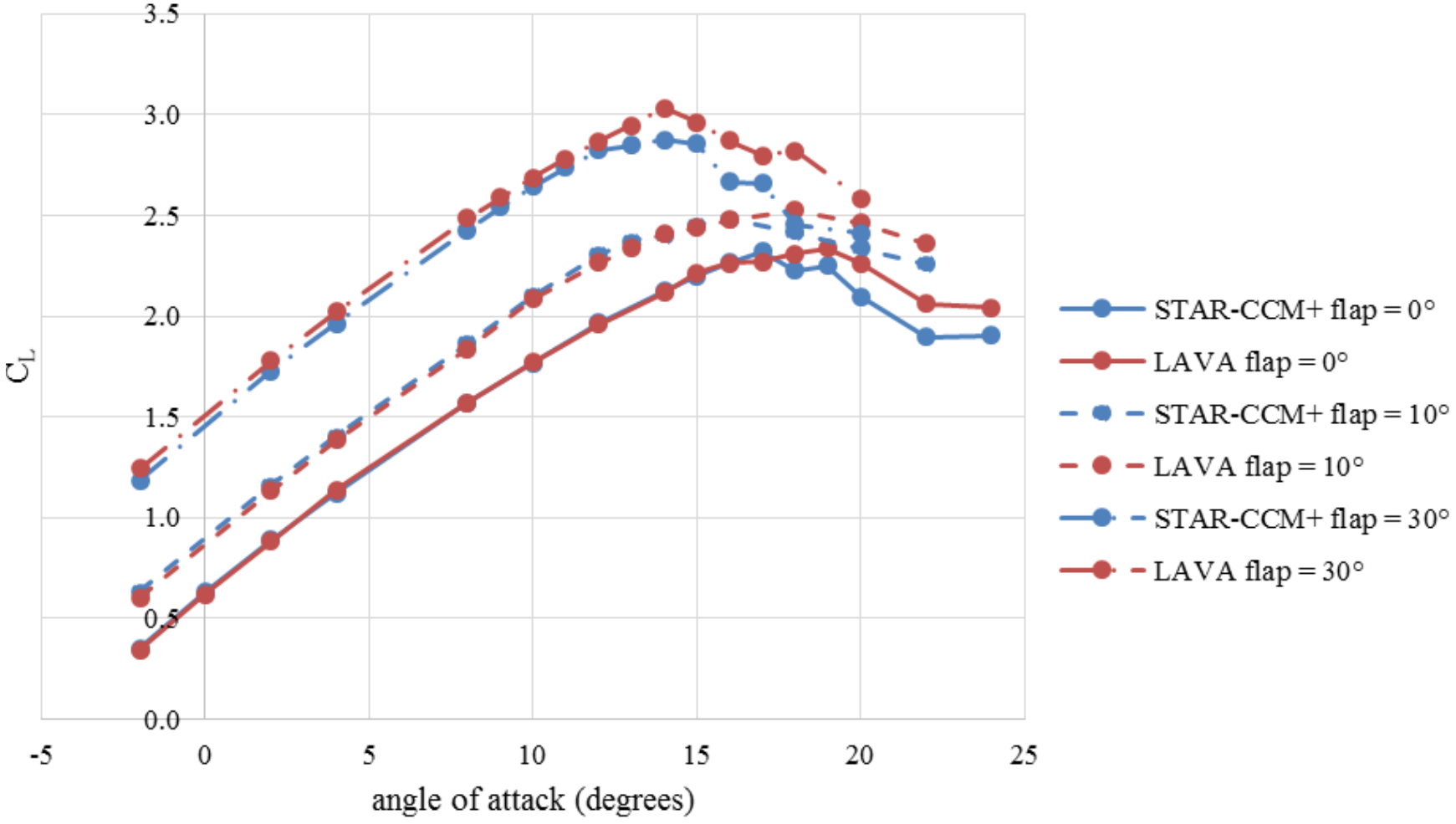

- Lift dependency on flap deflection
  - lift increases with increase in flap defection angle
  - Angle of attack for maximum lift decreases with increase in flap deflection
- Differences in solver
  - lift at high angle of attack
  - Increase in discrepancy with increase in flap deflection angle at linear region

Result – Angle of attack sweep

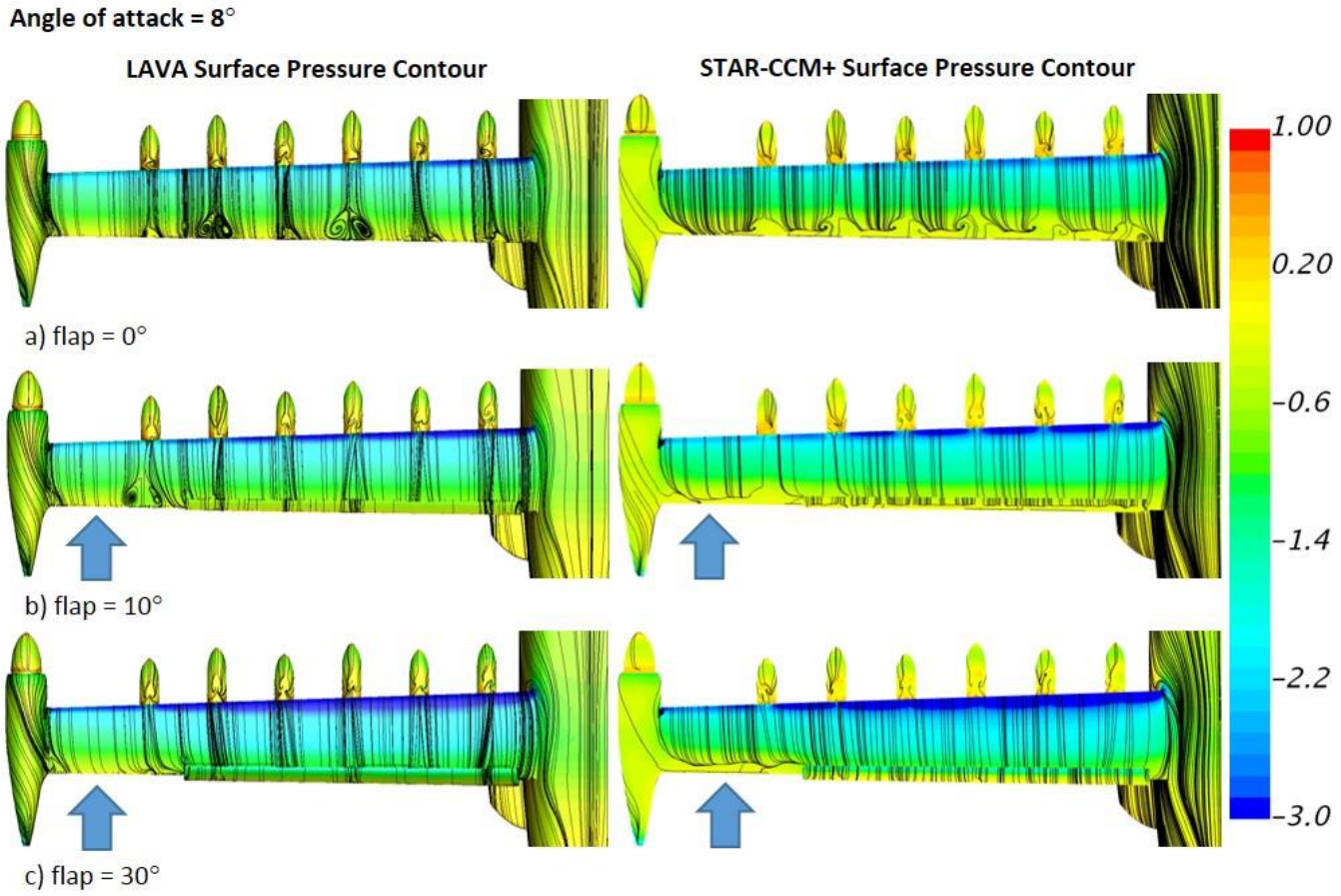

- Increase in solution discrepancy in lift with increase in flap deflection angle at linear region
- STAR-CCM+ solution show flow separation at outboard wing that is not show in LAVA for 10° and 30° flap deflection

Result – Angle of attack sweep

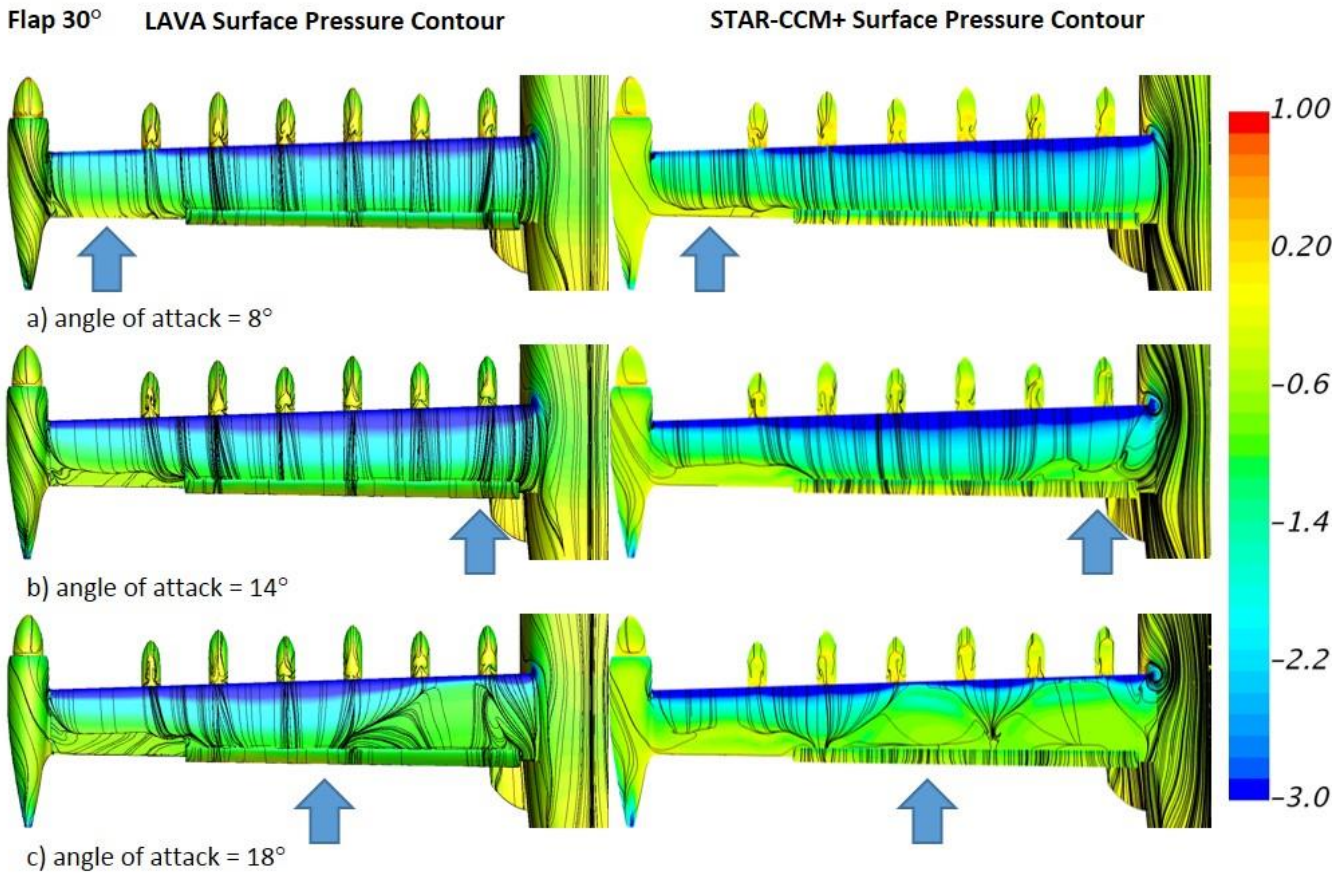

- Increase in solution discrepancy in lift at high angle of attack
- STAR-CCM+ solution show larger region of separated flow at higher angle of attack compared to LAVA

Result – Angle of attack sweep

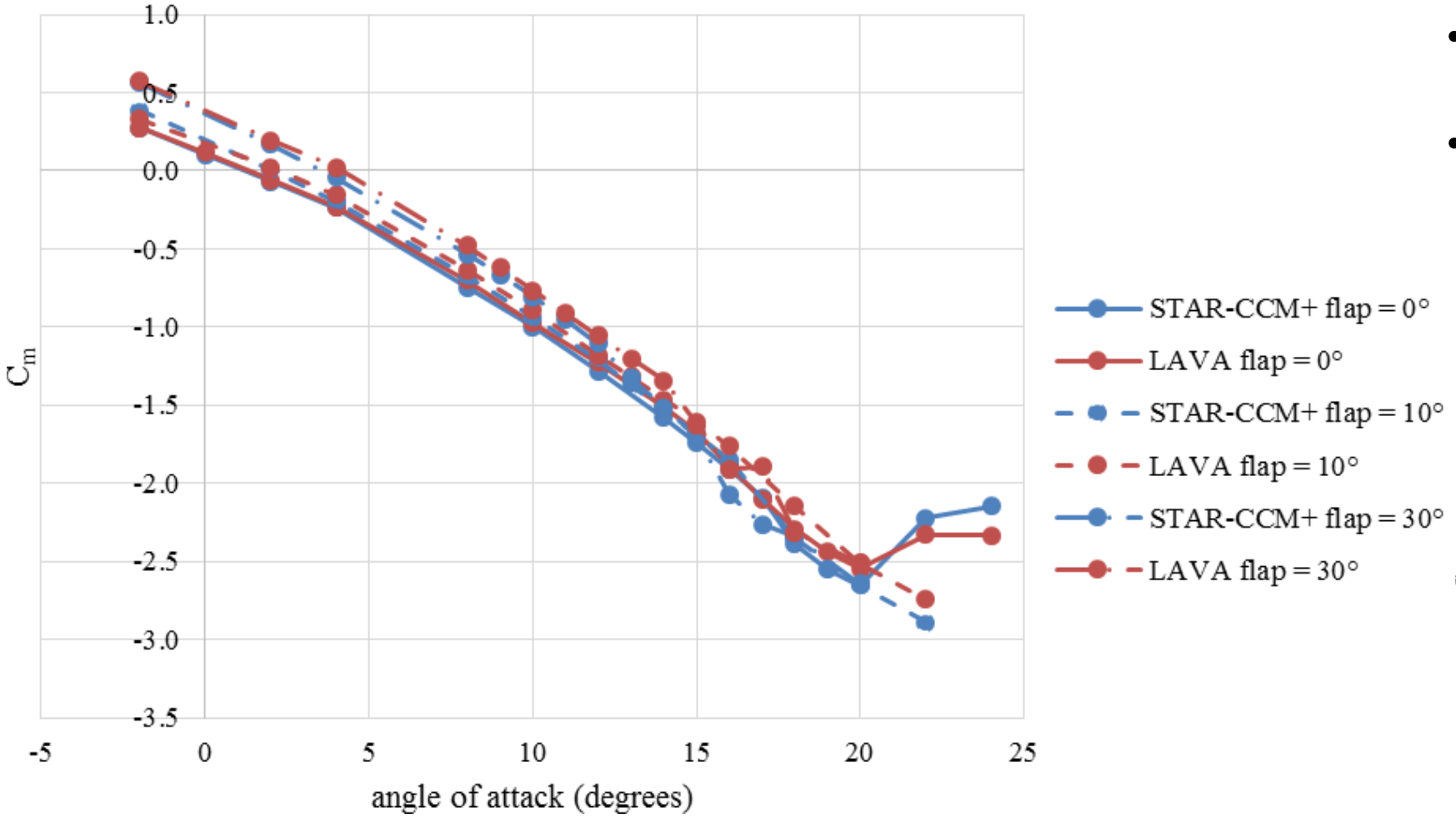

- Higher pitching moment with higher flap deflection angle
- Sharp increase in pitching moment for 0° flap angle at 20° angle of attack

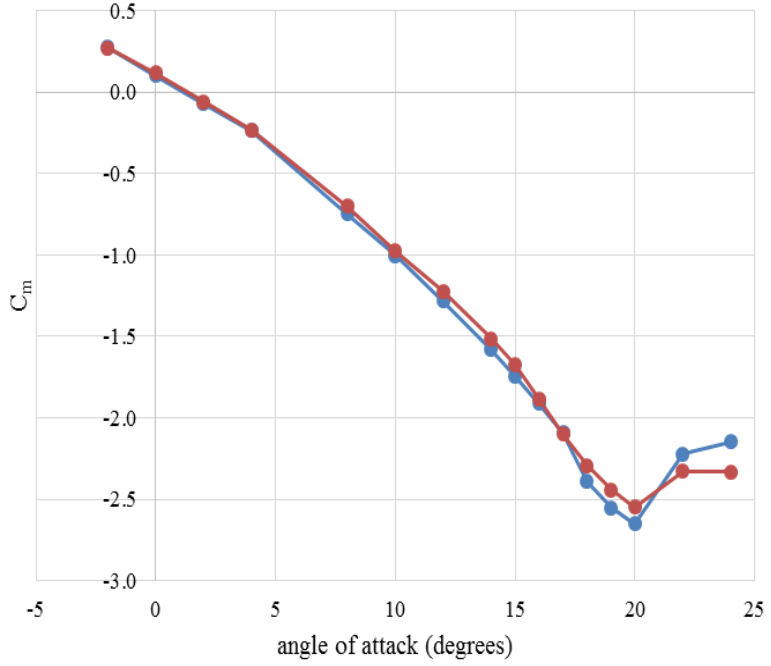

Result – Angle of attack sweep

Angle of attack = 22°, surface pressure contour

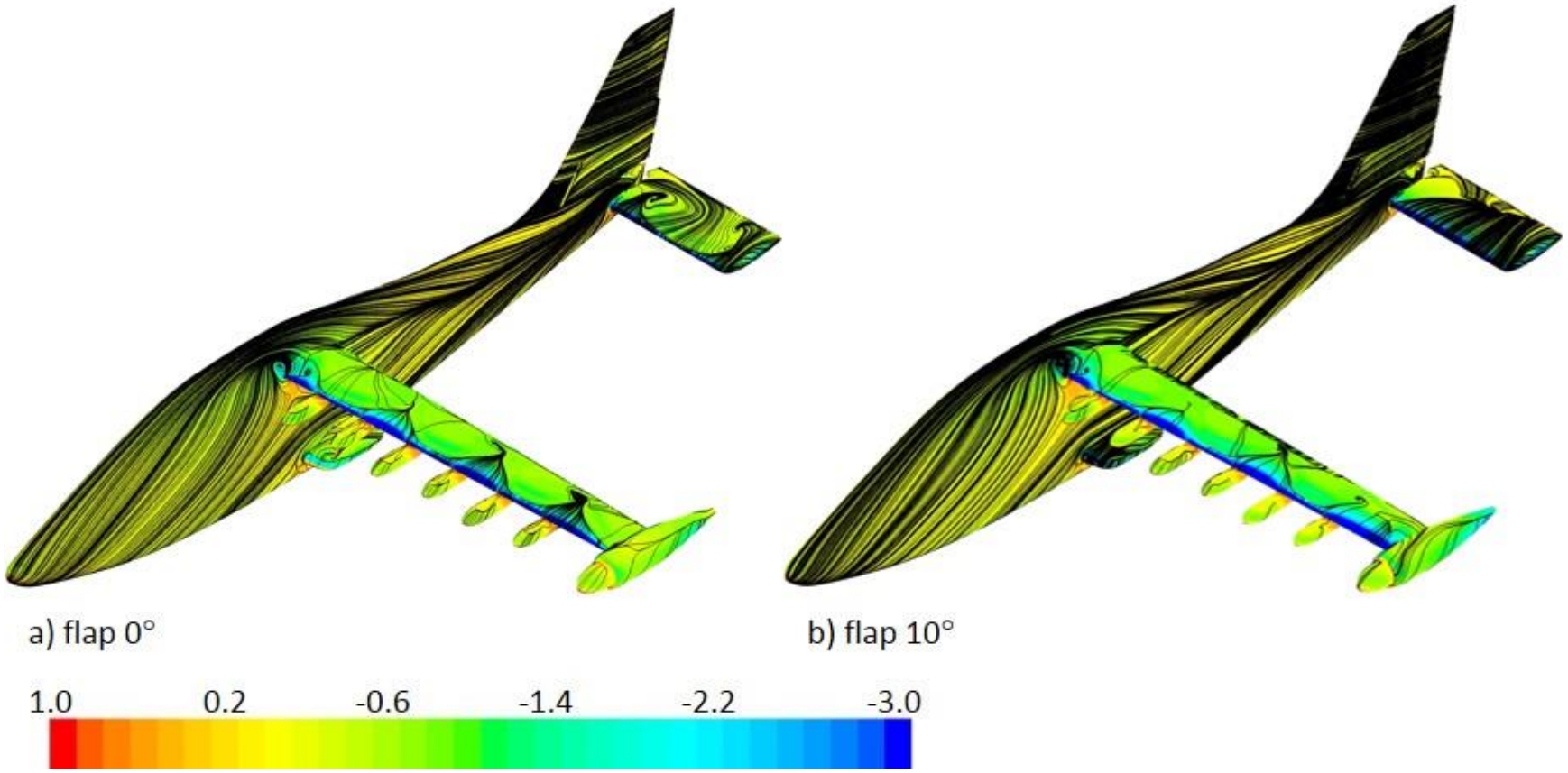

- Large flow separation shown on the upper surface of stabilator for 0° flap deflection configuration
- Flow separation shown on the upper surface of stabilator on 10° flap deflection configuration located to inboard and trailing edge

Result

- Grid Refinement Study
- Angle of attack sweep
- Sideslip angle sweep

Result – Sideslip angle sweep

- 3 flap settings – 0° (cruise) , 10° (take-off), 30° (landing)
- Control surfaces in neutral position (no deflection)

	Flap = 0°	**Flap = 10°**	**Flap = 30°**
Altitude, ft	8000	2500	2500
Mach	0.233	0.149	0.139
Density, slug/ft^3	1.8628E-3	2.20782E-3	2.20782E-3
Static pressure, lbf/ft^2	1571.9	1931.9	1931.9
Static temperature, K	272.3	283.2	283.2
Coefficient of viscosity, slug/ft/s	3.57532E-7	3.68708E-7	3.68708E-7
Reynolds number	1.32E6	9.875E5	9.21E5

Result – Sideslip angle sweep

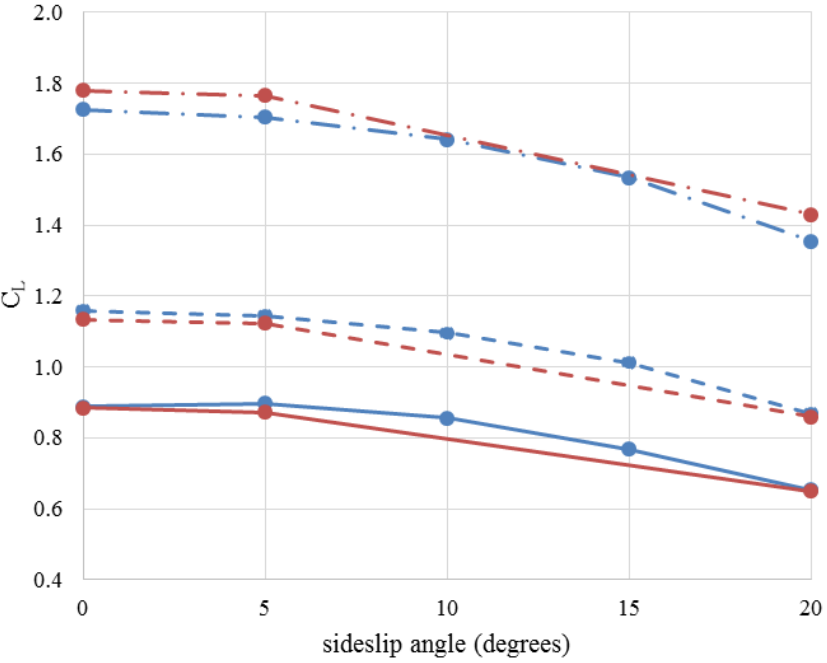

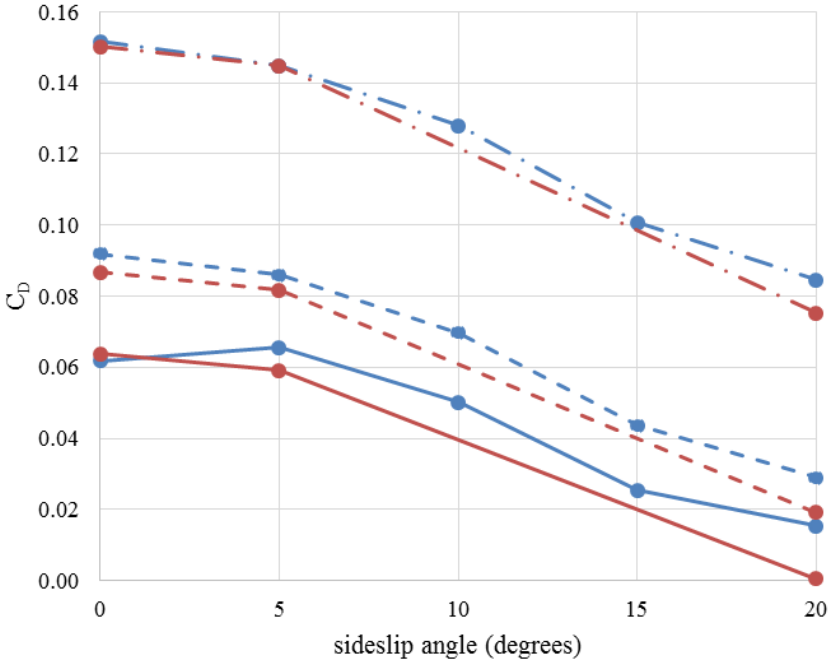

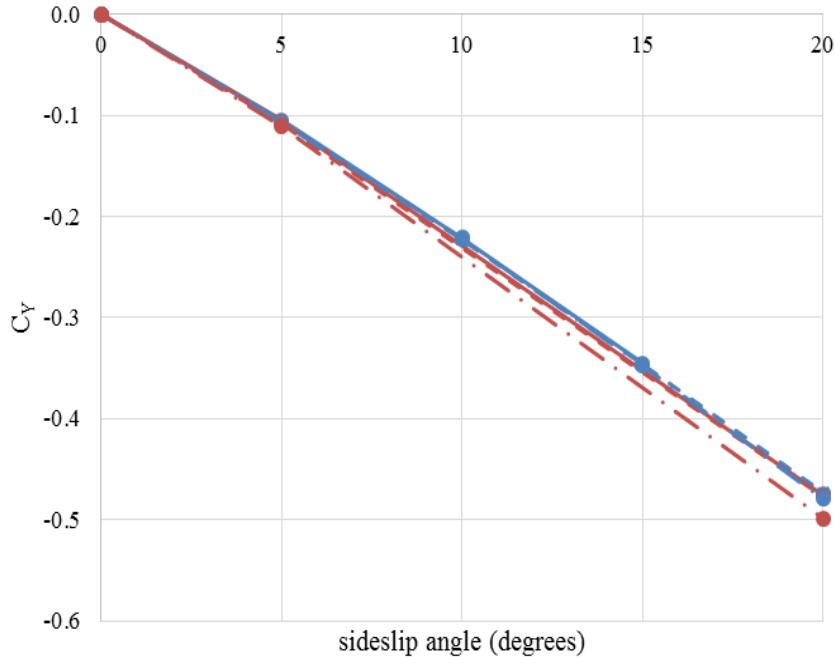

- Lift, drag, side forces all decrease with increasing sideslip angle
- Drag decreasing because it is in stability axis (increases when computed in wind axis)

Result – Sideslip angle sweep

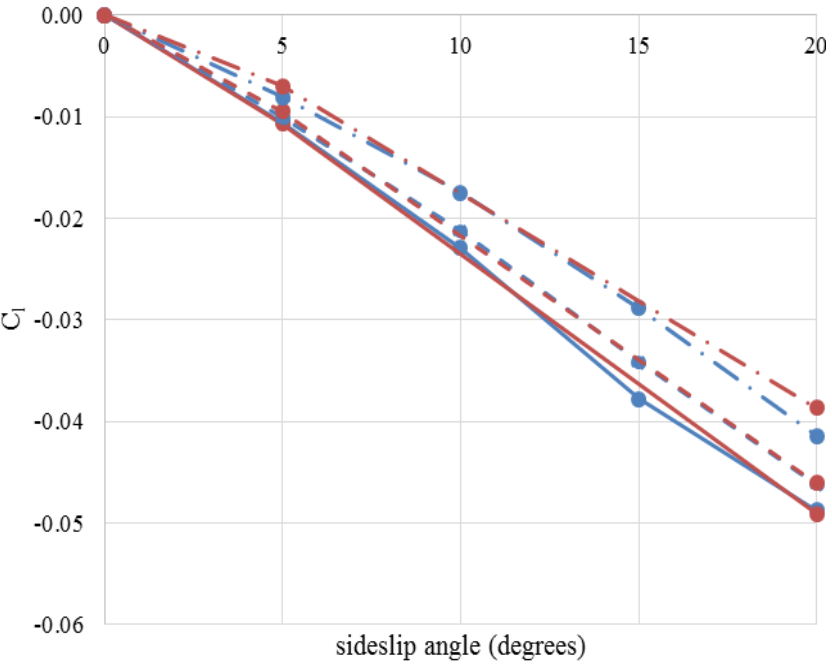

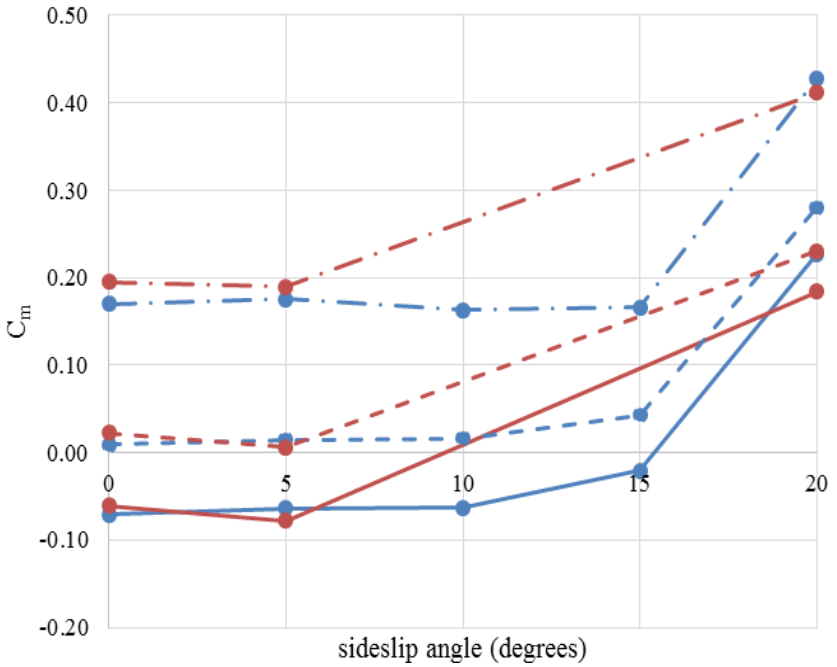

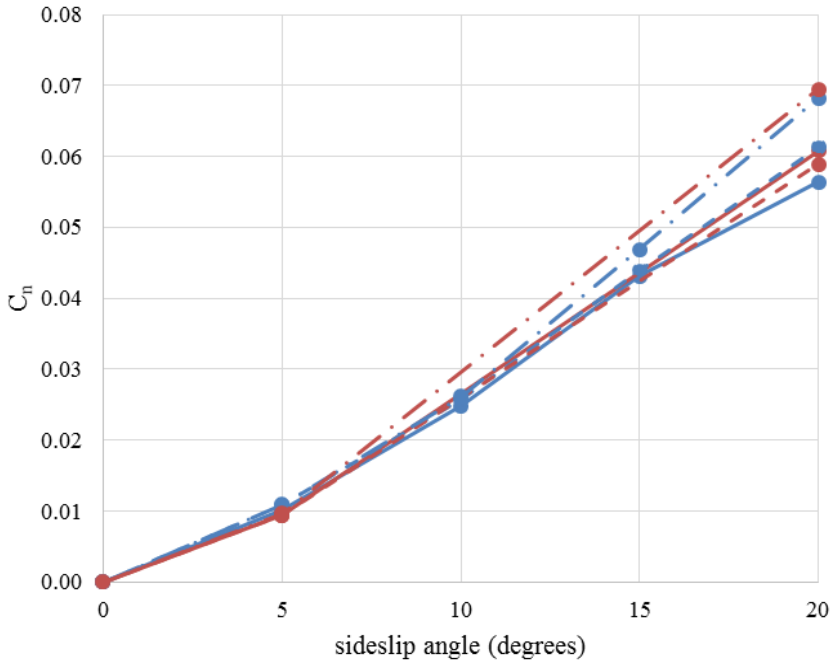

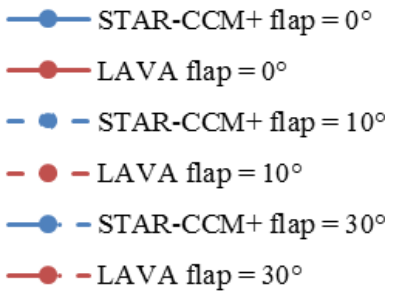

- Rolling moment - 30° flap produces least amount of rolling moment
- Pitching moment - sharp increase in at 15° for all flap deflections
- Yawing moment - 30° flap produces least amount of rolling moment

Result – Sideslip angle sweep

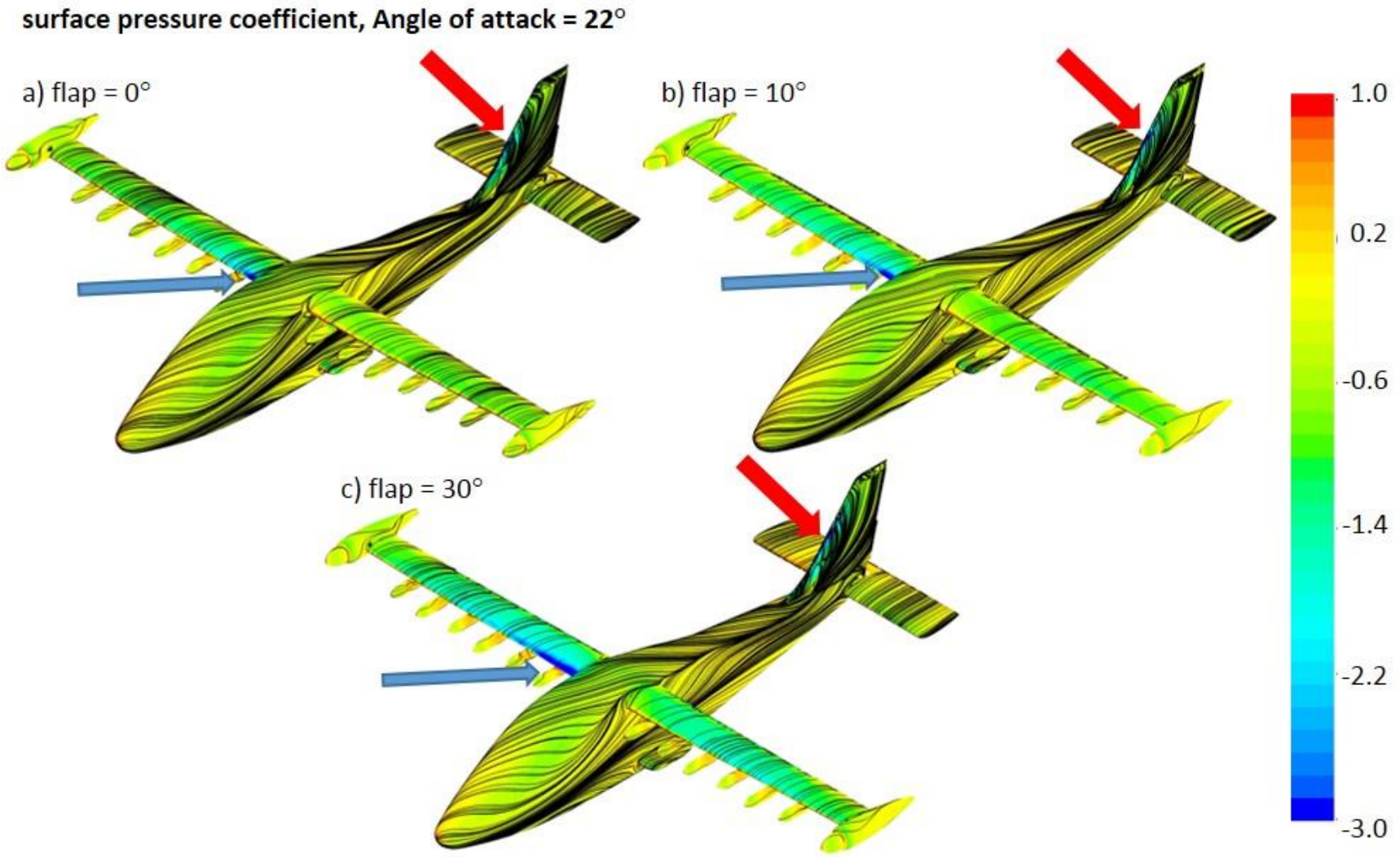

- Increasing separation at leading edge of right wing root with increasing flap deflection
- Separated region at the leading edge of rudder

Conclusion

- Unpowered X-57 MOD-III configuration analyzed
- Angle of attack sweep and sideslip angle sweep presented
- STAR-CCM+ and LAVA solution comparison
  - flow visualization show that solution compare well at low angle of attack
  - Difference in predicted separation behavior at higher angle of attack

QUESTION?